Scientific Reports

https://doi.org/10.1038/s41598-026-36741-6

Article in Press

Kinetic, equilibrium, and thermodynamic study of Methylene Blue adsorption on orange peel biochar prepared by microwave-assisted pyrolysis

Received: 5 August 2025

Accepted: 16 January 2026

Published online: 11 February 2026

Cite this article as: Correa-Abril J., Cabrera E.V., Robles N. *et al.* Kinetic, equilibrium, and thermodynamic study of Methylene Blue adsorption on orange peel biochar prepared by microwave-assisted pyrolysis. *Sci Rep* (2026). https://doi.org/10.1038/s41598-026-36741-6

Jhonny Correa-Abril, Elvia V. Cabrera, Nilo Robles, J. L. López Terán & Ullrich Stahl

Kinetic, Equilibrium, and Thermodynamic Study of Methylene Blue Adsorption on Orange Peel Biochar Prepared by Microwave-Assisted Pyrolysis

Jhonny Correa-Abril[1], Elvia V. Cabrera[1], Nilo Robles[1,2], J. L. López Terán[1] and Ullrich Stahl[1*]

[1]Universidad Central del Ecuador, Facultad de Ingeniería Química, Grupo de Investigación en Alimentos, Compuestos Orgánicos, Materiales, Microbiología aplicada, y Energía - ACMME. Enrique Ritter s/n y Bolivia, Quito, Ecuador.

[2]Instituto de Investigación Geológico y Energético - IIGE, Quito EC-170518, Ecuador.

* Correspondence: ustahl@uce.edu.ec

Abstract:

This study presents a sustainable approach for Methylene Blue (MB) dye removal using pristine, non-activated biochar derived from orange peel waste via Microwave-Assisted Pyrolysis (MAP). The key novelty lies in the systematic comparison of the biochar's adsorption performance under both pH-controlled (constant pH 4) and unregulated pH conditions, demonstrating that pH regulation is essential for optimizing adsorption efficiency. The resulting biochar exhibited a high fixed carbon content (60.89 %), an alkaline surface (Point of zero charge (pH_{pzc}) = 11.20, ZPotential = 0.1 mV @ pH 9), and oxygenated functional groups. Best MB removal of 83 % was achieved at pH 4, despite the expected electrostatic repulsion. Kinetic studies showed the best fit with the Elovich model, indicating a heterogeneous surface. The Langmuir isotherm accurately described the equilibrium data, revealing a maximum adsorption capacity (q_{max}) of 20.57 mg g^{-1} under pH-controlled conditions, representing an 83 % increase over the 11.24 mg g^{-1} obtained in the unregulated scenario. Thermodynamic analysis confirmed the process is spontaneous ($\Delta G° < 0$), endothermic ($\Delta H° = +4.88$ kJ mol^{-1} at constant pH), and governed by physisorption mechanisms, including hydrogen bonding and $\pi-\pi$ interactions. This work demonstrates that pristine orange peel biochar generated via MAP is a highly effective adsorbent and highlights the critical impact of pH control on improving adsorption capacity and elucidating the dominant physisorption mechanisms.

Keywords: Orange Peel, Microwave assisted pyrolysis, Biochar, Adsorption dynamics, Methylene Blue

Introduction

The rapid industrialization and urbanization in recent decades have generated challenges in water quality management. In this context, the textile industry stands out as a significant contributor, discharging large volumes of industrial effluents containing considerable amounts of synthetic dyes. Global annual dye production exceeds 700,000 tons, of which approximately 280,000 tons are discharged into water bodies through industrial effluents, making the textile industry responsible for about 20 % of global industrial wastewater production. Up to 80 % of these dye-polluted industrial wastewaters in most low and middle-income countries are released without treatment, leading to severe risks for human health and aquatic ecosystems, as many are toxic, mutagenic, and carcinogenic[1–3].

Methylene Blue (MB), a cationic dye (Fig. S1), is among the most widely applied synthetic dyes, with extensive applications in textile dyeing, paper coating, temporary hair colorants, and medical use. Even at concentrations as low as 1 mg L^{-1}, MB can cause a noticeable coloration to water bodies, affecting photosynthetic activity, leading to decreased oxygen levels and biodiversity. The dye's molecular structure grants it high stability and resistance to biodegradation, resulting in prolonged persistence in aquatic environments[4].

Traditional methods for treating dye-contaminated wastewater include coagulation - flocculation, membrane filtration, chemical oxidation, photocatalysis, and biological treatments. However, these methods often face challenges such as high operational costs, generation of harmful by-products, and inefficiencies in treating recalcitrant dyes[5,6].

Conventional adsorbents like activated carbon demonstrate excellent dye removal capabilities but are often associated with high production costs and environmental concerns. As a result, there is a growing interest in developing sustainable adsorbent materials[7].

Biochar (BC), produced through the pyrolysis of biomass under oxygen-limited conditions, is emerging as a promising alternative[8]. Its desirable characteristics such as a high surface area, well-developed pore structure, abundant surface functional groups and stability make it an effective adsorbent. Moreover, BC production aligns with circular economy principles by converting waste materials into valuable products, benefiting from relatively low production costs. Among potential waste biomass feedstocks, orange peel (OP) has emerged as a promising precursor for BC production. The global citrus processing industry generates over 12 million tons of OP waste annually, with limited current valorization options[9]. This abundant availability ensures a stable, low-cost feedstock supply.

OP's inherent characteristics, including high lignocellulosic content (approximately 50–70% by weight), natural porosity, and surface functional groups (particularly pectin and cellulose), contribute to the development of BC with enhanced adsorption properties. Furthermore, its low ash and high volatile matter content make it suitable for thermochemical conversion processes[10–12].

The BC production method significantly influences its physicochemical properties and, consequently, its adsorption performance. Microwave-assisted pyrolysis (MAP) represents a significant advancement over conventional heating methods. The unique direct heating mechanism of microwave irradiation results in rapid, uniform internal heating of the biomass, translating to shorter reaction times (typically minutes instead of hours) and reduced energy consumption (40–80% lower than conventional heating). This can lead to enhanced pore development and superior surface functionality in the resulting BC[13–15]. The environmental benefits of MAP include generating significantly fewer greenhouse gas emissions compared to conventional pyrolysis and reducing the overall carbon footprint of BC production. The technology's scalability and potential for continuous operation make it particularly attractive for industrial applications[16].

Despite growing interest in BC-based adsorption systems, many knowledge gaps remain. Specifically, the influence of MAP conditions on the physicochemical properties of OP-derived BC (BC-OP) and its MB removal performance remains poorly understood. The literature related to MAP, OP, and MB adsorption is scarce, although reports exist concerning different approaches, such as BC generation for catalyst support or the adsorption of other dyes[17,18].

Crucially, previous studies have often overlooked the systematic comparison of adsorption efficiency when the solution pH is actively regulated versus when it is allowed to drift naturally, especially for materials exhibiting high pH_{pzc}.

Our work provides a novel contribution by systematically investigating the adsorption of MB onto pristine, non-activated BC produced from OP waste via MAP, with a specific focus on comparing its performance under pH-controlled versus unregulated conditions, quantifying the improvement in adsorption capacity and providing detailed mechanistic insights into the non-electrostatic forces governing the process at optimal pH.

In this study, we investigated the adsorption capacity of MB in synthetic waters, employing a batch system and pristine BC, synthesized from OP using MAP. The BC-OP was rigorously characterized using physicochemical, structural, and morphological techniques. The effect of

pH in two scenarios (regulated and unregulated), the adsorbent dose, the initial adsorbate concentration, and the temperature were analyzed. The experimental data were interpreted using kinetic models and adsorption isotherms, and the thermodynamic parameters' enthalpy (ΔH°), entropy (ΔS°), and Gibbs free energy (ΔG°) were also determined to assess the feasibility of the adsorption process.

2. Materials and methods

2.1. Materials

OPs were obtained as waste from orange juice production in a central market in Quito, Ecuador. For the experiments, MB ≥ 82 %, sodium hydroxide ≥ 98 % (NaOH), and hydrochloric acid 37 % (HCl) were utilized, all acquired from Sigma Aldrich. All solutions were prepared using ultrapure water (Type 1)

2.2. Preparation of the raw material

The OPs were dried at room temperature and subsequently ground using a cutting mill (Retsch, SM300) with a 4 mm mesh screen at a speed of 800 rpm. Afterwards, the raw material was sieved, separating particles sized between 2.00 and 2.38 mm for further processing.

2.3. Obtaining BC-OP via MAP

The synthesis parameters were selected based on a previously established protocol described in Correa et al., and other relevant studies in this field [17], and were not a subject of optimization in this study. The MAP was conducted using a microwave oven (LG, MS1536GIR, 2.45 GHz, 1200 W), equipped with inverter technology, operating at a fixed power of 50 % (600 W) for a duration of 15 minutes. This specific combination of power and time was previously found to be effective for achieving a high degree of carbonization while retaining sufficient oxygenated functional groups on the biochar surface, yielding a material with favorable properties for adsorption applications. For this process, 100 g of OP were weighed into a quartz reactor measuring 58 mm in height and 43 mm in diameter with a cover[19]. The quartz reactor was covered during the entire 15-minute process, which physically prevents the ingress of atmospheric oxygen from the surrounding environment. The positive pressure generated internally by the evolving gases further ensures that air cannot enter the reactor (see Fig. S2).

2.4. Characterization of OP, BC-OP, and BC-OP-MB

Elemental analysis of OP and BC-OP was conducted using an Elementar Vario Macro Cube. Thermal stability and proximate composition were determined using a thermogravimetric analyzer (Mettler Toledo, TGA1). The samples were heated in an alumina crucible under an inert atmosphere (N_2) at a gas flow rate of 25 to 50 mL min^{-1}. The analysis was performed using a dynamic temperature ramp ranging from 20 to 100 °C at a heating rate of 20 °C min^{-1}, followed by an isothermal ramp at 100 °C for 10 minutes. Subsequently, a dynamic ramp from 100 to 700 °C was conducted at the same heating rate, and finally, an isothermal ramp at 700 °C for 20 minutes in an oxidizing atmosphere, with an air flow rate of 50 mL min^{-1}.

Furthermore, the surface area and pore volume of BC-OP were determined using BET analysis on a chemisorption instrument (Micromeritics, Autochem II 2920). Conductivity measurements (EC), pH, point of zero charge (pH_{pzc}), ZPotential (ZP) and Boehm titration were carried out following the methodology clearly described in[19].

FTIR spectrometry analysis (PerkinElmer, Spectrum Two) was conducted using potassium bromide (KBr) windows to collect spectral data in the range of 4000 - 400 cm^{-1} for the samples of OP, BC-OP, and BC-OP-MB. For the analysis of morphology and elemental composition, scanning electron microscopy (SEM) (Philips XL30 ESEM-FEG) equipped with Energy Dispersive X-Ray Spectroscopy (EDX) (EDAX Apollo XL-SDD) was employed.

2.5. Adsorption Experiments

The adsorption experiments were conducted in a batch system. The residual concentration of MB in each sample was determined using a UV-Vis spectrophotometer (Agilent, Cary 60) at a wavelength of 664 nm.

To determine the pH which generates the highest adsorption of MB on BC-OP, five solutions of 100 mL of MB with an initial concentration of 100 mg L^{-1} were prepared across a pH range of 2 to 10 in intervals of 2. To each solution, 1.0 g of BC-OP was added, and the mixtures were stirred at 200 rpm for 60 minutes. In order to maintain the pH of the solutions, NaOH and HCl were added at varying concentrations.

Once the pH that resulted in the highest adsorption (pH 4) was established, subsequent studies on the effects of adsorbent dose, contact time, adsorbate concentration, and thermodynamics were conducted using two different procedures:

Procedure one (constant pH): The solution pH was kept constant throughout all experiments using NaOH and HCl solutions at different concentrations.

Procedure two (unregulated pH), the pH was not regulated after the initial preparation and was allowed to drift naturally.

All experiments employed continuous stirring at 200 rpm unless stated otherwise, and all experimental work was carried out in duplicate.

To study the effect of adsorbent dose on the adsorption process, 0.5, 1.0, 1.5, 2.0, and 3.0 g of BC-OP were weighed and added to 100 mL of a 100 mg L^{-1} MB solution, which was stirred ~~at 200 rpm~~ for 60 minutes. This study was conducted following both procedures one and two.

For the study of the effect of contact time on the adsorption process, 1.0 g of BC-OP was weighed and added to 100 mL of a 100 mg L^{-1} MB solution, maintaining stirring for 15, 30, 60, 120, and 180 minutes, respectively, following procedure one and repeated using procedure two, where 2.0 g of BC-OP was used to study the effect of contact time.

To study the effect of MB concentration on the capacity of adsorption (q_e), solutions of MB were prepared at 100 mL with concentrations of 50, 100, 200, 300 and 500 mg L^{-1}, and 1.0 and 2.0 g of BC-OP were added, respectively, stirring for 60 minutes at a temperature of 293 K.

The thermodynamic study was conducted following the same procedures one and two from the MB concentration study, but varying the temperature to 278, 308, and 323 K, respectively. The temperature was measured using a FLUKE Ti 450 thermal camera.

2.6. Data Analysis and Evaluation

The removal capacity of MB before and after the adsorption process was calculated from the data obtained from UV-Vis using equations (1) and (2).

$$\%\, Removal = \frac{(C_o - C_t)}{C_o} * 100 \quad (1)$$

$$q = \frac{(C_o - C_t)}{W} * V \quad (2)$$

Where: q (mg g^{-1}) is the adsorption capacity, C_0 (mg L^{-1}) is the initial concentration of MB, C_t (mg L^{-1}) is the concentration of MB after the adsorption process, W (g) is the mass of the adsorbent, and V (mL) is the volume of the solution.

To evaluate the adsorption kinetics, the nonlinear models of pseudo-first order (PFO), pseudo-second order (PSO), and Elovich were employed[19].

The equations used in the pseudo-first order and pseudo-second order models are shown in equations (3), (4) and the Elovich model in (5).

$$q_t = q_e\,(1 - e^{-k_1 t}) \quad (3)$$

$$q_t = \frac{q_e^2 k_2 t}{1 + q_e k_2 t} \quad (4)$$

$$q_t = \frac{1}{\beta} ln(\alpha\beta t + 1) \quad (5)$$

Where: q_t (mg g^{-1}) is the amount of adsorbate adsorbed over time, q_e (mg g^{-1}) is the adsorption capacity at equilibrium, k_1 (min^{-1}) represents the PFO rate constant, k_2 (g mg^{-1} min^{-1}) represents the PSO rate constant, α (mg g^{-1} min^{-1}) is the initial adsorption rate, β (g mg^{-1}) is the constant related to the activation energy or the extent of occupied sites, and t (min) is the time[19].

To evaluate the adsorption equilibrium, the nonlinear models of the Langmuir (6), Freundlich (7), and Redlich-Peterson (8) isotherms were employed[19,20].

The dimensionless parameter derived from the Langmuir model, known as the separation factor R_L (9), allows for a more detailed analysis of whether the adsorption process is favorable.

$$q_e = \frac{q_{max} K_L C_{eq}}{1 + K_L C_{eq}} \quad (6)$$

$$q_e = K_F C_{eq}^{\frac{1}{n}} \quad (7)$$

$$q_e = \frac{K_{RP} C_{eq}}{1 + a_{RP} C_{eq}^{g}} \quad (8)$$

$$R_L = \frac{1}{1 + K_L C_0} \quad (9)$$

Where: q_{max} (mg g^{-1}) is the maximum adsorption capacity, K_L (L mg^{-1}) is the Langmuir affinity constant, C_0 (mg L^{-1}) is the initial concentration of the adsorbate, C_{eq} (mg L^{-1}) is the equilibrium concentration of the adsorbate, (mg g^{-1}) (L mg^{-1})$^{(1/n)}$) is the adsorption capacity at low concentration, 1/n represents the intensity of adsorption, K_{RP} (L g^{-1}) is the constant associated with the maximum adsorption capacity, a_{RP} (L mg^{-1}) is the constant related to the affinity between the adsorbate and the adsorbent, and g is the empirical exponent ($0 < g \leq 1$) which indicates a transition between Langmuir-type behavior ($g \rightarrow 1$) and Freundlich ($g \rightarrow 0$).

The thermodynamic parameters associated with the adsorption of MB were calculated using equations (10), (11), and (12).

$$\Delta G^0 = -RT\, ln\, K_c \quad (10)$$

$$\Delta G^0 = \Delta H^0 - T\Delta S^0 \quad (11)$$

$$ln\ K_c = (-\frac{\Delta H^0}{R})\frac{1}{T} + \frac{\Delta S^0}{R} \quad (12)$$

Where: R = 8.314 (J mol^{-1} K^{-1}) represents the universal gas constant, T (K) is the absolute temperature at which adsorption occurs, and K_c represents the dimensionless distribution coefficient. These values are determined graphically from the slope and intercept of the plot of ln K_c versus 1/T [20,21].

Finally in Fig. S3 a schematic of the synthesis process of BC-OP via MAP, characterization, and adsorption study of MB on BC-OP is shown.

3. Results and discussion

3.1. Characterization of OP and BC-OP

The adsorption of contaminants such as MB is strongly related to the surface chemistry of the adsorbent. In the present study, the physicochemical and morphological properties of OP and BC-OP were analyzed. Various analytical techniques were employed to determine these properties, and the results are presented in Table 1.

Table 1. Results of the physicochemical and morphological characterization of OP and BC-OP.

Parameter	**OP**	**BC-OP ***
Proximate analysis (wt. % on dry basis)		
Yield MAP (%)	-	22.33 ± 2.93
Moisture (%)	15.77	8.58
Volatile (%)	43.75	13.11
Fixed carbon (%)	32.02	60.89
Total ash (%)	8.46	17.42
Physicochemical properties		
C%	42.08 ± 1.44	60.84 ± 2.74
H%	6.46 ± 0.33	0.62 ± 0.07
O%	41.57 ± 1.83	19.19 ± 2.83
N%	1.44 ± 0.07	1.95 ± 0.06
H:C	0.15	0.01
O:C	0.99	0.32
C:N	29.22	31.20
Surface area (m^2 g^{-1})	-	6.22
Total pore volume *10^{-3} (cm^3 g^{-1})	-	3.10

pH	-	11.90
pH_{pzc}	3.38	11.20
ZP (mV) @ pH 9	-	-0.1 ± 0.3
EC (mS cm^{-1})	-	4.38

* MAP@600 W/15 min.

3.1.1. Proximate analysis

The yield of BC-OP via MAP was 22.33 %, which is comparable to the biomass pyrolysis results obtained by other researchers[22].

The comparison of the proximate analysis of OP and BC-OP conducted by TGA is presented in Table 1. It can be observed that the moisture content decreases from 15.77 % to 8.58 %, and similarly, the volatile matter decreases from 43.75 % to 13.11 %, while the ash content increases from 8.46 % to 17.42 %. These values indicate that OP enters the TGA with a higher moisture content than BC-OP, and during the thermogravimetric analysis, more volatiles are released from OP than from BC-OP obtained via MAP. This also implies that the MAP process did not fully carbonize the feedstock, which benefits the presence of functional groups on the BC-OP surface which can interact with dissolved adsorbates in fluids intended for removal. On the other hand, the increase in the inorganic fraction may enhance the ion exchange capacity of BC-OP, which is relevant in systems where ionic interaction is expected to be dominant, such as in the adsorption of cationic dyes[23,24].

These findings are consistent with previous studies that have reported similar results; an analysis on the characterization of OP feedstock found a moisture percentage of 10.45 %, while another study determined that the fixed carbon content in OP is 19.80 %[10,25,26].

The obtained thermograms are presented in Fig. 1. In the comparison of the results obtained for OP and BC-OP it is clearly observed in the DTG of Fig. 1 a) four characteristic peaks for the thermal decomposition of biomass, which consist of water loss and the decomposition of hemicellulose, cellulose, and lignin. In contrast, the DTG of Fig. 1 b) after the MAP process shows only two peaks, corresponding to water loss and the decomposition of residual lignin.

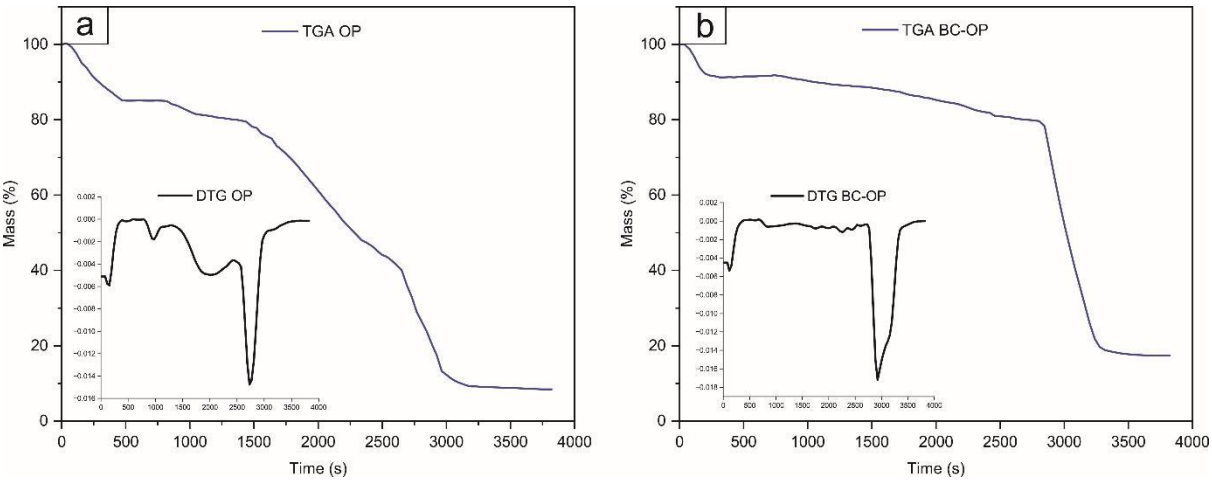

Fig. 1. TGA and DTG curve of a) OP and b) BC-OP. Experimental conditions: Inert atmosphere (N_2), dynamic temperature ramp ranging from 20 to 100 °C at a heating rate of 20 °C min^{-1}, isothermal ramp at 100 °C for 10 minutes, dynamic ramp from 100 to 700 °C, an isothermal ramp at 700 °C for 20 minutes with an air flow rate of 50 mL min^{-1}.

3.1.2. Elemental Analysis.

The results of the elemental analysis are shown in Table 1 in the physicochemical properties section. Significant changes in the chemical composition of OP after the MAP process can be observed, such as an increase in carbon content from 42.08 % in OP to 60.84 % in BC-OP. This indicates that the thermal treatment promoted the removal of volatile compounds, contributing to enhanced thermal and chemical resistance of the material, with a surface rich in organic compounds. On the other hand, a significant decrease in hydrogen content from 6.46 % to 0.62 % and in oxygen content from 41.57 % to 19.19 % was observed, indicative of the loss of volatile organic material, including CO_2 and H_2O, while maintaining a certain amount of oxygenated groups on the surface of the material. These results could positively influence the adsorption of cationic compounds and enhance the electrostatic interaction on the surface of BC-OP[27]. Regarding the nitrogen content, a slight increase from 1.44 % to 1.95 % was noted, which may be due to the transformation of nitrogenous compounds present in OP into more condensed and complex forms, a product of the Maillard reaction[28,29].

The mass ratios H:C and O:C of OP and their transformation into BC-OP decreased, indicating a dehydrogenation and aromatization of the material during pyrolysis. This resulted in a more condensed and stable structure, ideal for adsorption applications aimed at retaining organic compounds or heavy metals through physicochemical mechanisms. These

ratios serve as indicators of the quality of the obtained biochar[30,31]. Additionally, a slight increase in the N:C ratio was observed after the MAP, as previously mentioned[32].

The results of the BET surface area analysis for BC-OP, with particle sizes ranging from 2.00 to 2.38 mm, yielded a value of 6.22 $m^2\ g^{-1}$ and a total pore volume of $3.10 \times 10^{-3}\ cm^3\ g^{-1}$. The BC-OP has an average pore diameter of 1.26 µm, determined using the PoreVision software[33] (see Fig. S4). This diameter is significantly larger than that of a MB molecule (1.7 x 0.76 x 0.33 nm), suggesting that the biochar possesses an adequate capacity for adsorbing MB molecules, thereby facilitating their retention in wastewater treatment applications[32–34].

3.1.3. Determination of pH, pH_{pzc}, ZP and EC

The pH of OP was determined as 3.38, while the pH of BC-OP was 11.9. This elevated pH is a result of the ashes of BC-OP being released into the water, raising the pH, as well as the EC. As higher pyrolysis temperatures volatilize more biomass, more ashes remain, influencing pH and EC[35]. For EC a value of 4.38 mS cm^{-1} was found, which is in the range of values found in the literature, which oscillate between 0.4 and 54.2 mS cm^{-1} [36].

As the most important factor of sorption processes on biochar are the functional oxygen and nitrogen groups, determining the pH_{pzc} is of utmost importance. This parameter describes the surface polarity of the biochar. If the pH surrounding the biochar particle is lower than the pH_{pzc}, the surface is positively charged, while on a higher pH, the surface is deprotonated and thus, negatively charged. In the present case, it would be optimal to work at a pH higher than the pH_{pzc} determined, as the MB molecule is a cation (MB^+)[37]. Fig. S5 shows the pH_{pzc} value determined for BC-OP (11.20), which is in agreement with the results from Albalasmeh et al., 2020[38].

To further investigate the surface charge, the ZP was measured at pH 9, yielding a value of -0.1 mV (see Fig. S6). This result indicates that even at a pH below the pH_{pzc}, the biochar surface is essentially neutral to slightly negative, which can be attributed to the deprotonation of strong acidic functional groups like carboxylic acids.

3.1.4 *Boehm titration*

The Boehm titration is a simple method used for the quantitative analysis of oxygen functional groups of carbon materials. The results of the Boehm titration of BC-OP are shown in Table 2. The total acidity determined as 470.04 µmol g^{-1} can be separated into 221.65 µmol g^{-1} carboxylic groups and 248.39 µmol g^{-1} lactonic groups, which can interact in anionic form with cationic species like MB^+. The value for the phenolic groups found was negative, which can be explained as in Breen et al.[39], as a possible interaction with cations released

from the ash content of BC-OP. Thus, the amount of phenolic functional groups could not be determined. These data were obtained by applying the direct titration methodology. In Fig. S7 a schematic is shown illustrating the Boehm titration neutralization of oxygen functional groups according to their acidity using multiple bases with different pK_a.

Table 2. Boehm titration of oxygenated functional groups of BC-OP.

F. GROUP	**nCSF (μmol g^{-1})**
Carboxylic	221.65
Lactonic	248.39
Phenolic	-245.80
Total acids	470.04

3.1.5 Analysis SEM/EDX

The scanning electron microscopy (SEM) images are shown in Fig. 2 and Supplemental information 2 (S2). Comparing the micrograph of OP with that of BC-OP, significant changes resulting from the MAP process can be observed. In the image of OP, a relatively rough and compact surface is noted, with little porous structure, characteristic of natural lignocellulosic biomass, exhibiting low surface area[40].

For the BC-OP image, a highly porous surface is observed, featuring cracks and internal channels with a broad distribution of pore sizes. These characteristics indicate a structural reorganization induced by the removal of volatile components during MAP, which enhances accessibility to active sites on the surface of the material. The fractured texture and presence of pores are consistent with previous studies on biochars derived from agricultural residues, demonstrating that thermal treatment favors the development of more complex and stable porous structures[32,41].

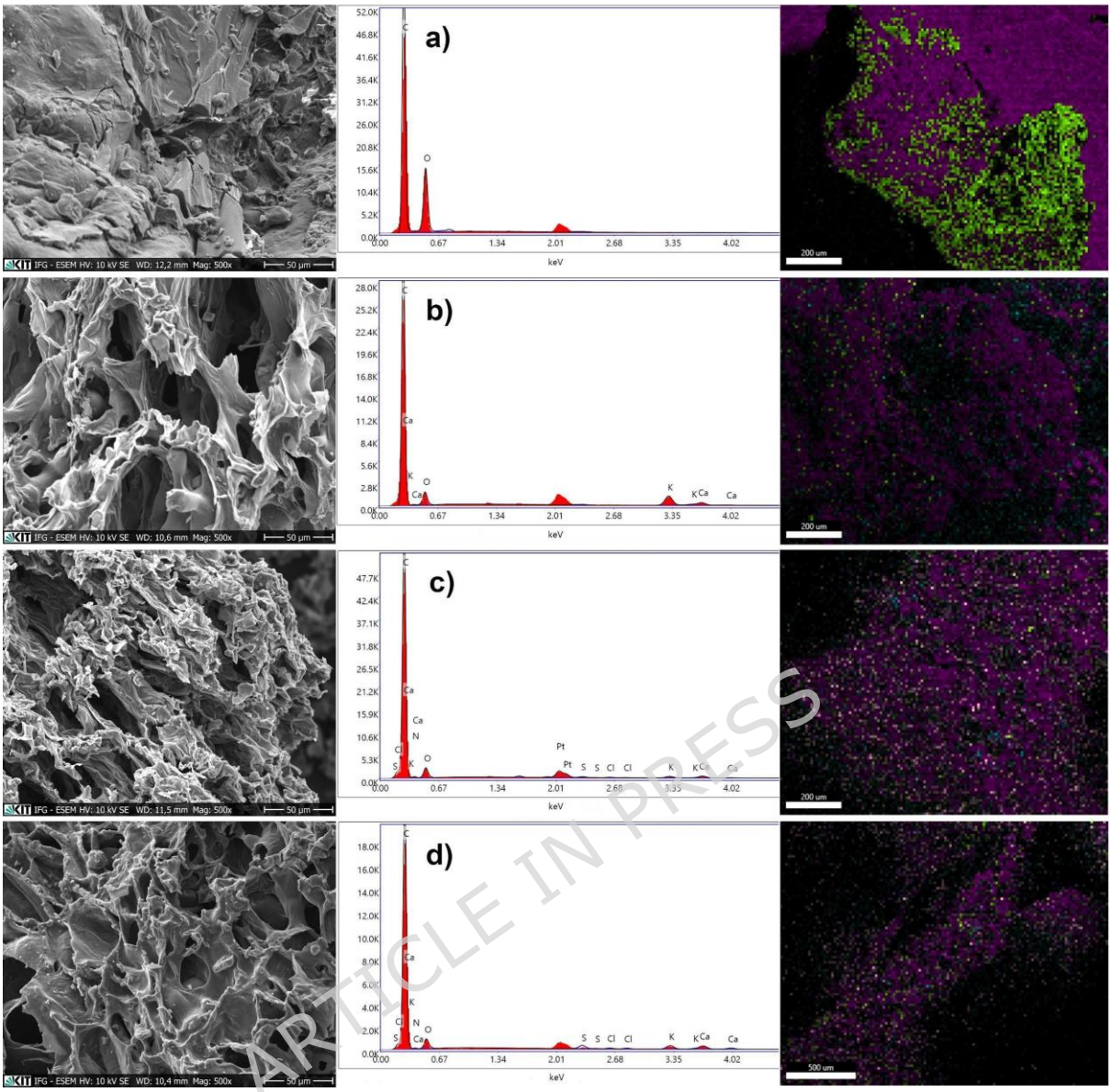

Fig. 2. SEM micrograph, EDX spectra and elemental mapping of a) OP, b) BC-OP, c) BC-OP-MB1.0 and d) BC-OP-MB0.5.

Analyzing the images of MB adsorption on BC-OP-MB1.0 (1.0 g of biochar in 100 mg L^{-1} MB solution) and BC-OP-MB0.5 (0.5 g of biochar in 100 mg L^{-1} MB solution), revealed changes in surface porosity and roughness compared to BC-OP. Both images show altered surface morphology, seemingly caused by the conditions during the MB adsorption process. In the results from the EDX analyses and elemental mapping, clear differences indicate the changes that occurred during the MB adsorption process on BC-OP compared to BC-OP and OP. Additionally, the presence of nitrogen, sulfur, and chlorine in the respective EDX spectra confirm the presence of MB on the surface of BC-OP, suggesting molecular interactions. Meanwhile, the relative decrease in potassium and calcium after adsorption could be related to the electrostatic competition between the metallic cations present in BC-

OP and the MB^{+} [5]. The complete quantitative results for the 4 samples are presented in the supplemental information S2.

3.1.6. FTIR spectra analysis

The FTIR spectra of OP and BC-OP are compared with those of BC-OP subjected to a MB adsorption process (BC-OP-MB) and are shown in Fig. 3. In the spectrum of OP, a broad absorption band is observed between 3500 and 3000 cm^{-1}, indicating the presence of stretching vibrations of -OH groups, characteristic of cellulose, pectin, hemicellulose, and lignin. The band at 2920 cm^{-1} is attributed to the stretching vibrations of C-H bonds from -CH_3 and -CH_2 groups. Additionally, the band at 1731 cm^{-1} identifies the stretching vibrations of carbonyl (C=O) groups present in organic compounds, including pectin, hemicellulose, and lignin. The absorption bands in the range of 1300 to 1000 cm^{-1} correspond to the stretching vibrations of C-O bonds from carboxylic acids, esters, alcohols, and pyranoses. When comparing the FTIR spectrum of OP with that of BC-OP, the same absorption bands are observed, albeit with slight changes in displacement and intensity, demonstrating the decomposition of certain surface groups during pyrolysis. The FTIR spectrum following the adsorption of MB in aqueous solution, referred to as BC-OP-MB, exhibited significant alterations in various bands, indicating that the functional groups on the surface of BC-OP actively participated in the adsorption of MB[42].

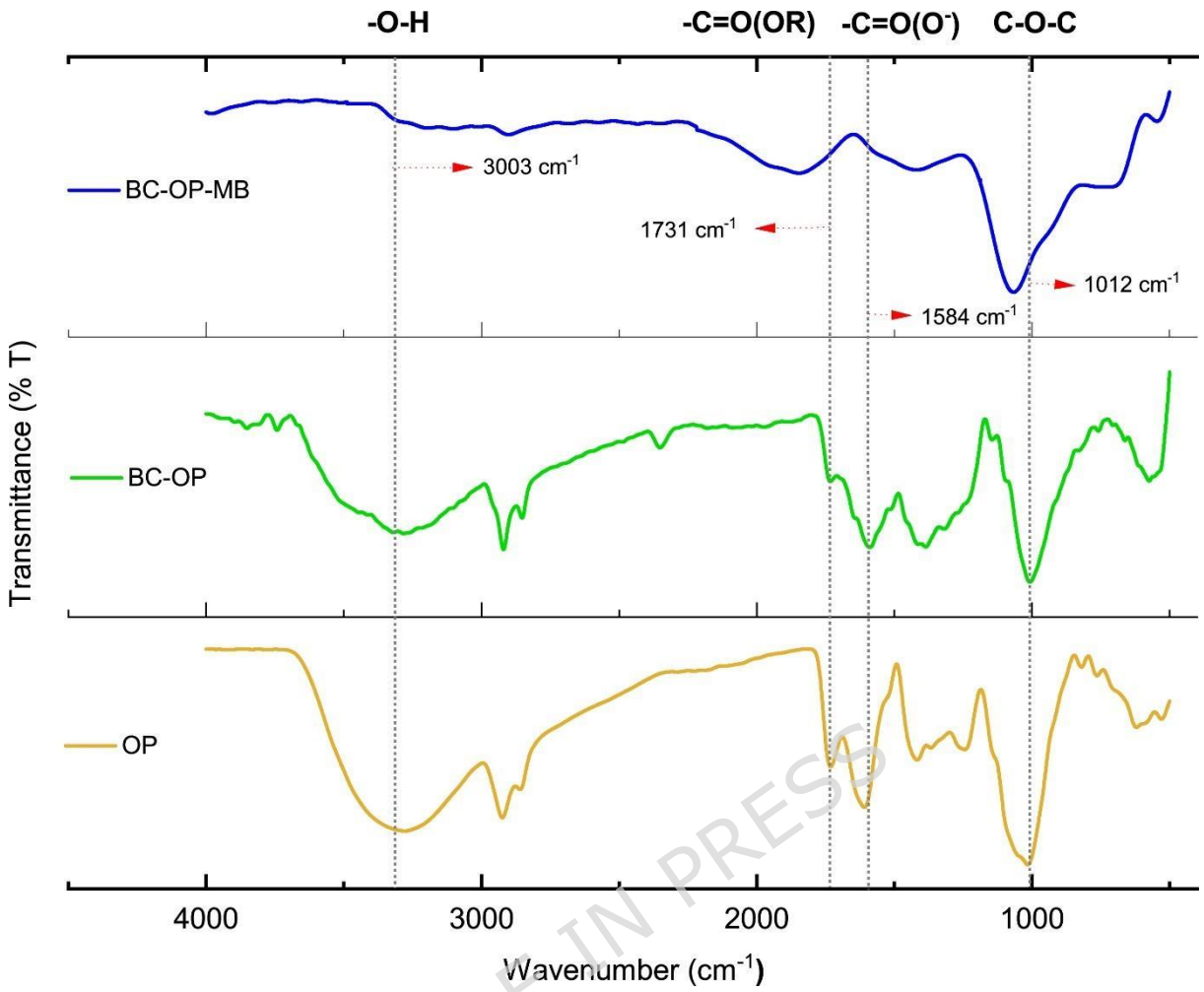

Fig. 3. FTIR spectra of OP, BC-OP and BC-OP-MB.

4. Adsorption study of MB on BC-OP

4.1. Effect of solution pH

The best adsorption percentage found was 83 % at pH 4 (see fig. 4). Given the high pH_{pzc} of BC-OP (11.2), electrostatic repulsion of the cationic MB^+ (pK_a = 3.8) might be expected to reduce adsorption at this moderately acidic pH. However, the strong removal observed suggests that non-electrostatic interactions, such as hydrogen bonding and π - π stacking / n-π interactions, are the primary drivers of adsorption. A more comprehensive explanation synthesizing the ZP results, thermodynamic parameters, and proposed physisorption mechanisms is described in Section 4.6.

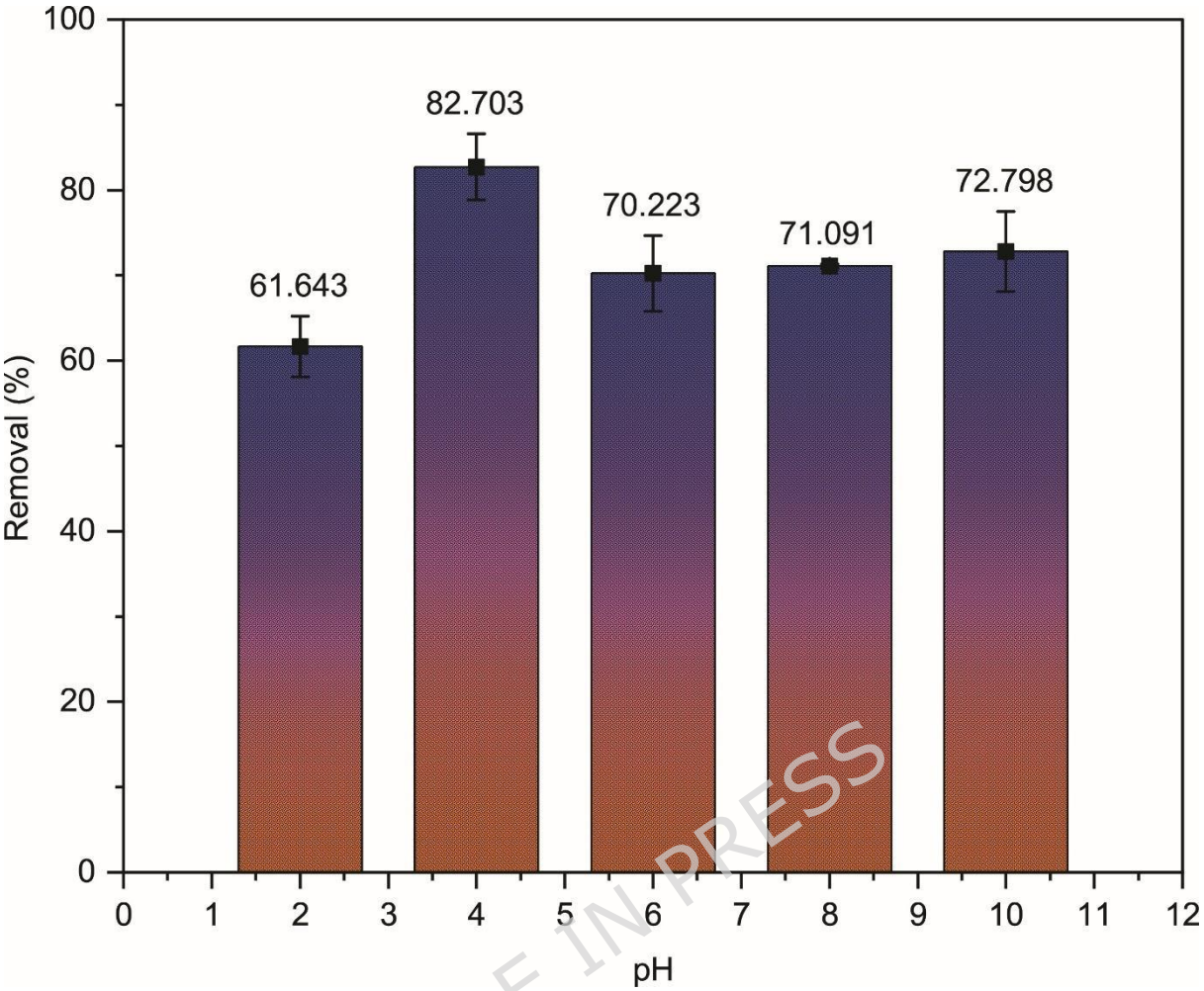

Fig. 4. Influence of pH on the percentage of adsorption of MB on BC-OP. Experimental conditions: pH range (2, 4, 6, 8, 10), BC-OP dose = 1g ; $V_{sol.}$ = 100 mL; C_0 MB = 100 mg L^{-1}; T = 293 K; stirring speed = 200 rpm; time = 60 min.

4.2. Effect of adsorbent dosage

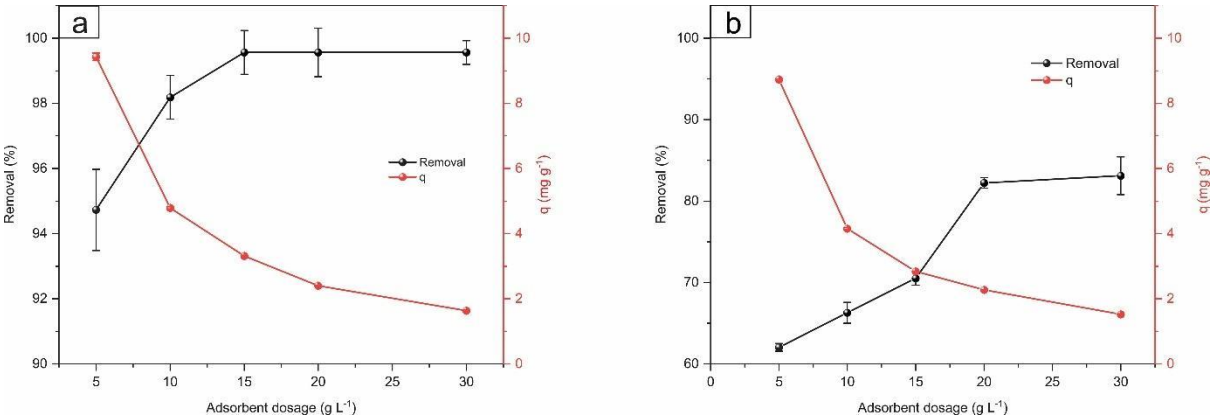

Fig. 5. Influence of adsorbent dosage of BC-OP on adsorption percentage: a) under constant pH conditions, b) without pH regulation. Experimental conditions: BC-OP dose = (5,

10, 15, 20 25, 30) g L^{-1}; $V_{sol.}$ = 100 mL; C_0 MB = 100 mg L^{-1}; T = 293 K; stirring speed = 200 rpm; time = 60 min.

Fig. 5 illustrates the relationship between the dosage of the adsorbent BC-OP (g L^{-1}) and the percentage of MB adsorption under constant pH conditions as well as without pH regulation at a concentration of 100 mg L^{-1} MB. According to Ho and McKay [43], a higher number of available active sites on BC-OP enhances interaction with MB, resulting in an increased adsorption capacity. This behavior is clearly observed in Fig. 5 a and b, at 10 (g L^{-1}) and 20 (g L^{-1}), respectively. At these adsorbent doses, the percentage of adsorption reaches a state of equilibrium. A notable difference between the conditions with constant pH and without regulation suggests that pH is a critical factor in the efficiency of the adsorption process. This study aimed to determine the differences between controlling or not controlling the pH during the MB adsorption process, as there are no reports related to this parameter for this type of material. The results depicted in Fig. 5 demonstrate that controlling the pH during the adsorption process is essential for optimizing interactions between the adsorbent and the adsorbate, facilitating the protonation or deprotonation of functional groups on the adsorbent [44,45].

4.3. Effect of contact time

To evaluate the effect of contact time on the adsorption of MB onto BC-OP, three kinetic models were employed: PFO, PSO, and Elovich. The results are presented in Fig. 6 and Table 3 which show that the Elovich model provides the best fit when the pH is constant, with an R^2 value of 0.991 and a Chi^2 of 0.123. This high R^2 value indicates that the model effectively captures the complexity of the adsorption process, suggesting that the surface of BC-OP is heterogeneous and that the active sites possess different activation energies throughout the adsorption process. The parameter α = 410.980 indicates a high initial adsorption capacity, while β = 1.318 suggests that the rate of adsorption decreases as the active sites become occupied[46]. In comparison to the Elovich model, the PSO model also demonstrates a good fit, with an R^2 value of 0.984 and a Chi^2 of 0.217. This suggests that the adsorption is largely governed by the occupation of multiple active sites[43]. However, the lower Chi^2 value in the Elovich model indicates that, although the PSO is suitable, it does not accurately describe the adsorption process in this system.

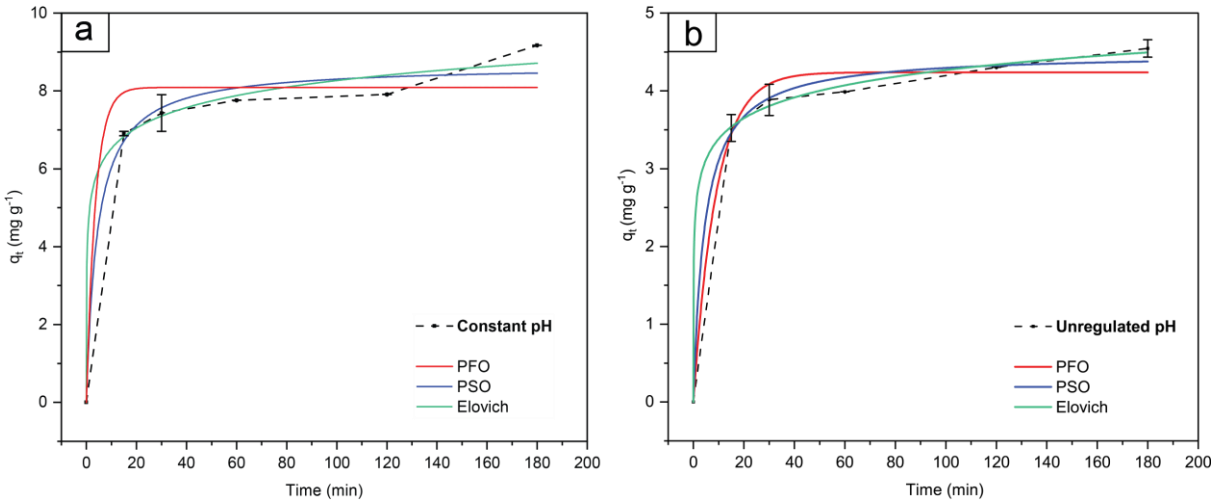

Fig. 6. Contact time for the adsorption process of MB onto BC-OP: a) under constant pH conditions, b) without pH regulation. Experimental conditions: a) BC-OP dose = 10 g L^{-1}, b) BC-OP dose = 20 g L^{-1}. a) and b): time 15, 30, 60, 120 and 180 min.; $V_{sol.}$ = 100 mL; C_0 MB = 100 mg L^{-1}; T = 293 K; stirring speed = 200 rpm.

In the case of the PFO model, the R^2 values for both constant pH and unregulated pH were lower, reaching 0.948 and 0.986, respectively, along with Chi^2 values of 0.706 and 0.051. This suggests that the model is not suitable for describing this adsorption process. These findings are consistent with the literature, which indicates that this model is less effective in systems where the interactions are more complex[47-49].

The comparison of results for constant pH and unregulated pH for the PSO model reveals that, when pH is controlled, the q_e reaches 8.663 mg g^{-1}, which is significantly higher than the value of 4.480 mg g^{-1}, obtained with unregulated pH.

The q_e values under unregulated pH conditions indicate that the BC-OP surface adapts to changing environmental conditions[50]. This finding suggests that the variability of pH affects the availability of active sites on the biochar[44].

Table 3. Adsorption kinetics parameters for MB in the BC-OP.

PFO				
Condition	**q_e (mg g^{-1})**	**k_1 (min^{-1})**	**Chi^2**	**R^2**
Constant pH	7.836	1.863	0.706	0.948
Unregulated pH	4.240	0.111	0.051	0.986

PSO				
Condition	**q_e (mg g^{-1})**	k2 **(g mg^{-1} $min)^{-1}$)**	**Chi^2**	**R^2**
Constant pH	8.663	0.026	0.217	0.984
Unregulated pH	4.480	0.050	0.017	0.995
Elovich				
Condition	**α (mg g^{-1} min^{-1})**	**β (g mg^{-1})**	**Chi^2**	**R^2**
Constant pH	410.980	1.318	0.123	0.991
Unregulated pH	253.510	2.600	0.004	0.999

4.4. Adsorption isotherm studies

The adsorption isotherm models of Langmuir, Freundlich, and Redlich-Peterson, shown in Table 4 and Fig. 7 were applied to study the equilibrium of the adsorption process of MB on BC-OP. The results obtained for the Langmuir model yielded q_{max} values of 20.57 mg g^{-1} for a constant pH and 11.24 mg g^{-1} for an unregulated pH, indicating that BC-OP has a significantly higher adsorption capacity in the constant pH scenario. This represents a substantial quantitative improvement (approximately 83 % increase) achieved solely by maintaining the optimum pH of 4. This key finding demonstrates that at a constant pH of 4, the adsorption process is heavily favored by the formation of stronger, targeted non-electrostatic interactions between the biochar and MB, a finding that addresses the necessity of defining optimal operating conditions for practical application[50,51].

Table 4. Isotherm parameters of MB adsorption on BC-OP.

Langmuir				
Condition	**q_{max} (mg g^{-1})**	**K_L (L mg^{-1})**	**Chi^2**	**R^2**
Constant pH	20.570	0.014	0.401	0.989
Unregulated pH	11.241	0.033	0.748	0.952
Freundlich				

Condition	K_F ((mg g^{-1}) (L mg^{-1})$^{(1/n)}$)	1/n	Chi^2	R^2
Constant pH	1.171	0.492	0.282	0.981
Unregulated pH	1.229	0.426	0.100	0.993
Redlich-Peterson				
Condition	K_{RP} (L g^{-1})	a_{RP} (L mg^{-1})	g	Chi^2	R^2
Constant pH	0.340	0.039	0.849	0.498	0.991
Unregulated pH	482.960	392.100	0.576	0.134	0.993

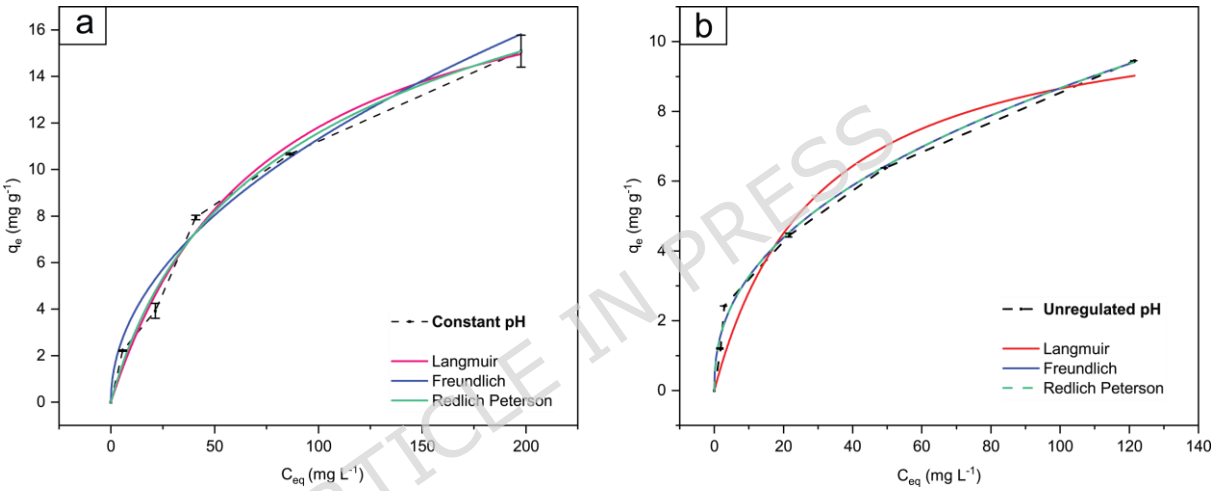

Fig. 7. Equilibrium isotherms of the adsorption process of MB on BC-OP for a) constant pH, b) unregulated pH. Experimental conditions: a) BC-OP dose = 10 g L^{-1}, b) BC-OP dose = 20 g L^{-1}. a) and b): C_0 MB = 50, 100, 200, 300 y 500 mg L^{-1}, V_{sol} = 100 mL; T = 293 K; stirring speed = 200 rpm; time = 60 min.

With the data obtained from the Langmuir model adjustment, at different concentrations of MB at constant pH and unregulated pH for BC-OP the following was obtained: the separation factor R_L is less than 1 in both scenarios presented in Table 5, indicating that adsorption is favorable under both conditions. A R_L value less than 1 suggests that the adsorption is spontaneous, while a R_L value greater than 1 indicates that the adsorption is not spontaneous[52].

Table 5. Results for the separation factor R_L for the Langmuir model at different concentrations of MB at constant pH and unregulated pH for BC-OP.

Separation Factor R_L					
C_0 (mg L^{-1}) MB	**50**	**100**	**200**	**300**	**500**
Constant pH	0.597	0.426	0.270	0.198	0.129
Unregulated pH	0.377	0.377	0.132	0.092	0.057

The Freundlich model describes the adsorption process on heterogeneous surfaces[53]. The results of the study reveal important information about the adsorption capacity of BC-OP and the influence of pH regulation. The K_F values are similar under both pH conditions, suggesting a comparable adsorption capacity. The values of 1/n are found to be between 0 and 1 in both cases, confirming that the adsorption process is favorable[54].

The Redlich-Peterson model combines characteristics of both Langmuir and Freundlich, showing a good fit in both scenarios. However, the model suggests more complex interactions in the unregulated scenario, as evidenced by the high values of K_{RP} and a_{RP}[55].

In Fig. 7, the adsorption trends in both scenarios are observed. The results from the models indicate that BC-OP exhibits a better adsorption capacity at constant pH conditions. The q_{max} values are notably higher in this scenario, suggesting that maintaining a constant pH of 4 maximizes the availability of active sites and enhances the adsorption interactions between BC-OP and MB.

The reported q_{max} of BC of OP and other biomasses for MB adsorption are shown in Table 6.

Table 6. Comparison of the q_{max} of BC-OP and other adsorbents of MB and other dyes.

Reference	**Biomass Used**	**Synthesis / Pyrolysis Conditions**	**Pollutant / Application**	**Result (q_{max} or Main Finding)**
Hanafi et al. (2024)[56]	Blend: Orange Peel + Watermelon Rind	Microwave assisted activation with $ZnCl_2$.	Crystal Violet (CV) Methylene Blue (MB)	q_{max} 137.8 mg g^{-1} (CV) 200.7 mg g^{-1} (MB)
Lam et al. (2017)[42]	Orange Peel	2 step MAP + chemical activation (KOH / NaOH).	Malachite Green (MG)	q_{max} 28.5 mg g^{-1}

Amin et al. (2019)[57]	Orange Peel vs. Banana biomass	Conventional slow pyrolysis at 800 °C.	MB	q_{max} > 90 mg g^{-1} (Orange peel was superior to Banana). Pseudo-second-order kinetics.
Jawad et al. (2024)[18]	Blend: Orange Peel + Watermelon Rind	Microwave activation (800 W, 20 min) with H_3PO_4.	MB	q_{max} 225.2 mg g^{-1} (pH 10, 25 °C). Endothermic and spontaneous process.
Gurer et al. (2021)[58]	Bitter Orange Peel	Chemical activation with $ZnCl_2$ or H_3PO_4 carbonized at 450 or 550 °C.	MB	q_{max} 90.58-108.9 mg g^{-1}
Nuryana et al. (2020)[33]	Coconut Shell	MAP (550/650 W, 15-25 min). No chemical activation.	MB	q_{max} 0.6875 mg g^{-1}
Our study	**Orange Peel**	**MAP (600 W, 15 min)**	**MB**	**q_{max} 20.57 mg g^{-1}**

4.5. Thermodynamics study.

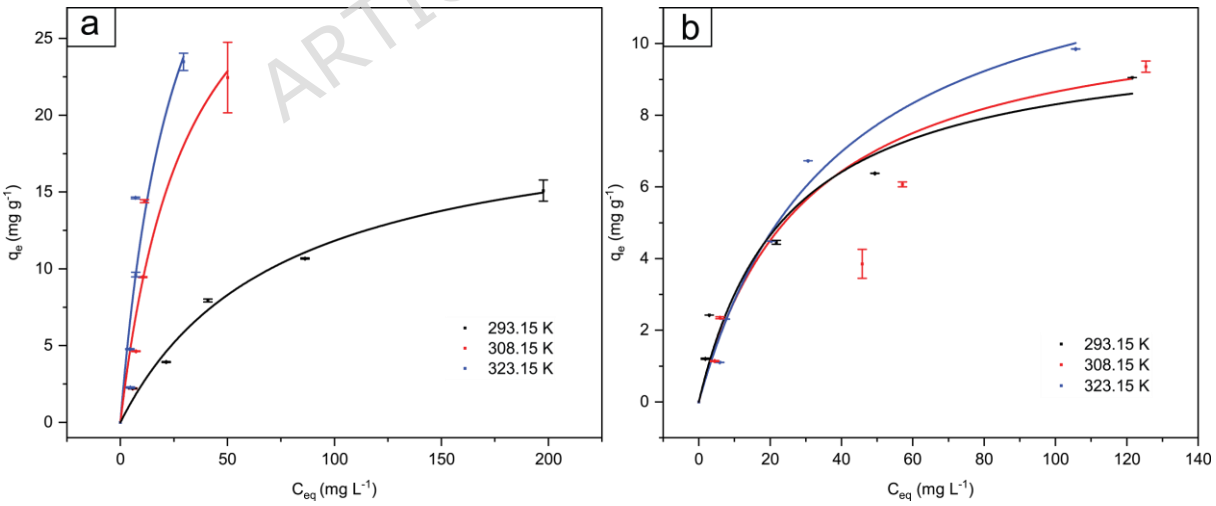

Fig. 8. Effect of initial concentration of MB on the adsorption capacity of BC-OP at various adsorption temperatures for a) constant pH and b) unregulated pH. Experimental conditions: a) BC-OP dose = 10 g L^{-1}, b) BC-OP dose = 20 g L^{-1}, a) and b): T = 293, 308, 323 K, C_0 MB = 50, 100, 200, 300 y 500 mg L^{-1}.; V_{sol} = 100 mL; stirring speed = 200 rpm; time = 60 min.

Table 7. Thermodynamic parameters.

Unregulated pH			
Temperature (K)	**ΔG^0 (kJ mol^{-1})**	**ΔH^0 (kJ mol^{-1})**	**ΔS^0 J mol^{-1} K^{-1}**
293.15	-32.40	2.21	118.14
308.15	-34.26		
323.15	-35.94		
Constant pH			
Temperature (K)	**ΔG^0 (kJ mol^{-1})**	**ΔH^0 (kJ mol^{-1})**	**ΔS^0 J mol^{-1} K^{-1}**
293.15	-32.24	4.88	126.41
308.15	-33.92		
323.15	-36.05		

The thermodynamic parameters of the adsorption process were determined by studying the system at temperatures of 293.15, 308.15, and 323.15 K. Fig. 8 shows the effect of initial concentration of MB on the adsorption capacity of BC-OP carried out at various adsorption temperatures for constant and unregulated pH. These data are very important for the prediction of the mechanism of adsorption. This was done by relating the Gibbs free energy (ΔG°) to the Van't Hoff equation (12), which also allowed for the estimation of the thermodynamic parameters of enthalpy (ΔH°) and entropy (ΔS°)[21]. Table 7 shows that the values of ΔG° at all temperatures studied are negative and decrease as the temperature increases in both scenarios. This indicates that the adsorption of MB on BC-OP is a spontaneous and thermodynamically favorable process at higher temperatures[5,59]. This behavior is characteristic of endothermic processes, as observed in this study. The positive values of ΔH° of 2.21 kJ mol^{-1} for the unregulated pH and 4.88 kJ mol^{-1} for the constant pH system) confirm that the adsorption is endothermic[60,61]. This endothermic nature suggests that an input of energy is required for the process to occur, which may be due to the desolvation of the MB^+ cation and the reorganization of the adsorbent-adsorbate interface[61].

Furthermore, the magnitude of ΔH° is clearly below 40 kJ mol^{-1}, which rules out a mechanism based on chemisorption and supports a process dominated by physisorption[62], where electrostatic interactions, π - π interactions, n- π interactions, Van der Waals forces, and hydrogen bonds prevail.

Likewise, the values of ΔS° are positive 118.14 J mol^{-1} K^{-1} and 126.41 J mol^{-1} K^{-1}, respectively, indicating an increase in molecular disorder at the adsorbent-adsorbate interface. This increase in entropy can be attributed to the release of solvate water molecules from both the MB^+ ion and the surface functional groups of BC-OP during the adsorption process, which enhances the degrees of freedom in the system and favors the spontaneity of the process[63,64].

4.6. Proposed mechanism of adsorption of MB onto BC-OP

The results of this research are schematically presented in Fig. 9, supported by findings obtained through various characterization techniques, as well as kinetic, equilibrium, and thermodynamic studies. In the FTIR analysis, the spectra of BC-OP and BC-OP-MB showed significant changes in the adsorption bands, suggesting interactions between the surface functional groups present on the surface of BC-OP and the dye. The SEM-EDX analysis revealed characteristic peaks of nitrogen, sulfur, and chlorine in the BC-OP-MB, elements corresponding to the structure of the MB molecule which were not detected in the EDX spectra of BC-OP and OP.

The results from the Boehm titration corroborate the presence of oxygenated functional groups on the surfaces of BC-OP, which facilitate hydrogen bonding, n-π interactions, and electrostatic interactions that are crucial for the removal of cationic contaminants like MB^+.

The overall adsorption mechanism of MB onto BC-OP is dominated by physisorption, supported by multiple lines of evidence:

1) Thermodynamic evidence: The low magnitude of the positive ΔH° values (+4.88 kJ mol^{-1} for constant pH) confirms that the process is endothermic and strongly supports a physisorption mechanism, as ΔH° values are clearly below 40 kJ mol^{-1}.
2) Surface charge mitigation: The pH study demonstrated maximal removal at pH 4, despite the high pH_{pzc} (11.20). This is explained by the ZP measurement at pH 9, which yielded a value of -0.1 mV. This near-neutral result suggests that the surface

positive charge below the pH_{pzc} is weak or negligible, thereby minimizing electrostatic repulsion and allowing non-electrostatic forces to dominate.

3) Non-electrostatic interactions: The predominant interactions include hydrogen bonding, π - π stacking and n- π interactions. Hydrogen bonding is formed between the oxygen containing groups (e.g. -OH and -COOH) on the BC-OP surface and the nitrogen atoms in MB molecules. Furthermore, the aromatic structures of MB enable π - π stacking with the aromatic regions of the biochar carbon matrix, while lone pair electrons on oxygen atoms in functional groups can participate in n-π interactions with the π orbital system of MB.

This detailed mechanistic understanding, particularly the identification of hydrogen bonding and π - π interactions as the primary adsorption drivers at a seemingly unfavorable acidic pH of 4, constitutes a significant novelty of this work. It challenges the simplistic assumption that electrostatic repulsion should dominate below the high pH_{pzc} (11.20), revealing that controlled pH conditions effectively enhance non-electrostatic pathways, thereby optimizing the utility of MAP-derived OP biochar.

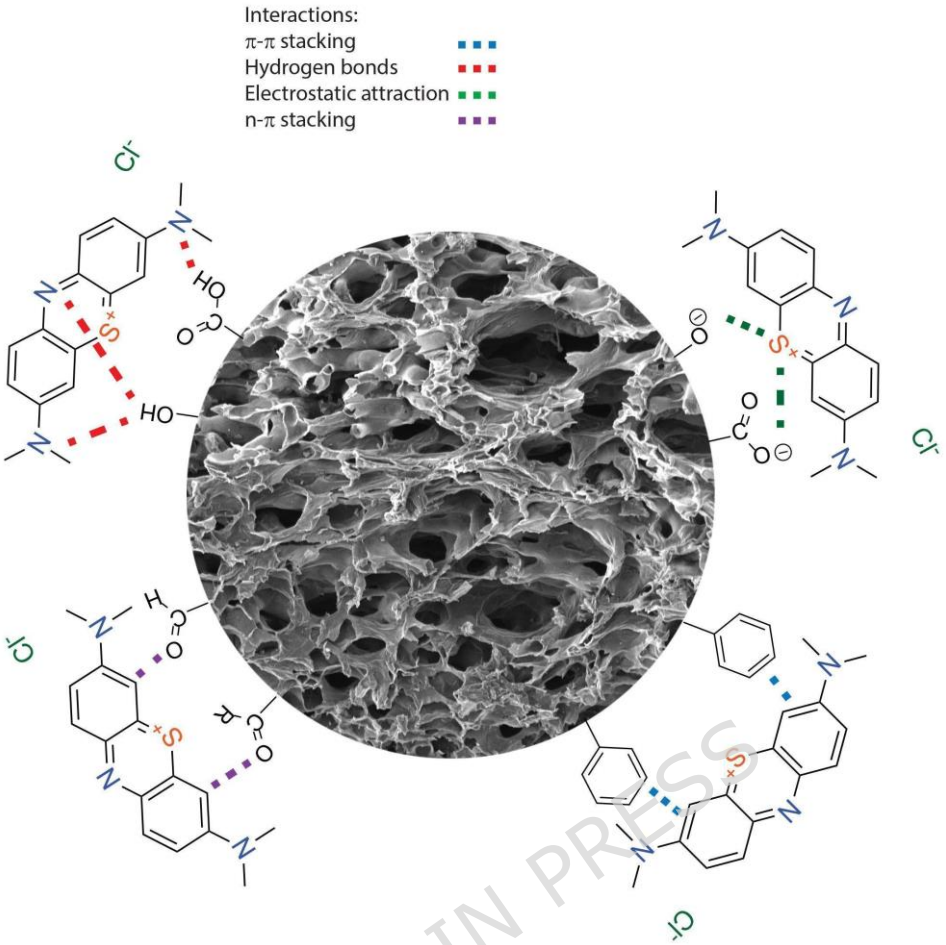

Fig. 9. Proposed adsorption mechanism of MB onto BC-OP.

A critical factor in the utilization of any adsorbent is its stability and the potential for leaching secondary pollutants[65]. The biochar studied herein is derived from clean agricultural waste, and its synthesis does not involve harsh chemicals, contributing to its inherently clean nature. The high ash content (17.42%) is responsible for the elevated pH of 11.90, which may affect the solubility of various inorganic constituents. Future research will quantify the leaching of inorganic cations, such as potassium (K) and calcium (Ca), to further evaluate environmental safety.

Although the fundamental characteristics of this biochar suggest it is a sustainable material, comprehensive safety testing remains essential in future investigations. Such assessments will target the leaching of dissolved organic carbon (DOC), heavy metals, and polycyclic aromatic hydrocarbons (PAHs) under different water conditions. These studies will be required to establish the environmental suitability of the biochar for practical applications in water treatment.

6. Conclusion

This study successfully demonstrated the formation of BC-OP from OP via MAP and evaluated its efficacy as an adsorbent for MB removal from aqueous solutions. The MAP process yielded 22.33 % BC-OP, leading to a significant increase in carbon content from 42.08 % to 60.84 % and a decrease in hydrogen and oxygen content, indicative of enhanced thermal and chemical resistance and material aromatization. The resulting BC-OP exhibited an alkaline pH of 11.90 and a pH_{pzc} of 11.20, alongside a suitable average pore diameter of 1.26 μm for MB molecule adsorption. Furthermore, Boehm titration and FTIR analysis confirmed the presence of oxygenated functional groups (predominantly carboxylic and lactonic groups), which are crucial for interacting with cationic contaminants like MB^+. Regarding the adsorption performance, the solution pH was identified as a critical factor, with a maximum MB adsorption of 83 %, achieved at an initial pH of 4. This suggests that despite the biochar's high pH_{pzc}, a moderately acidic environment promotes hydrogen bond, π–π and n–π interactions. Increasing the adsorbent dose enhanced the adsorption capacity, reaching equilibrium at 10 g L^{-1} under constant pH conditions and at 20 g L^{-1} without pH regulation, highlighting the importance of pH control for optimal efficiency. Kinetic studies revealed that the Elovich model provided the best fit for MB adsorption under constant pH conditions (R^2 = 0.991), indicating a heterogeneous surface with varying activation energies. The PSO model at the same conditions showed a good fit (R^2 = 0.984), suggesting that the adsorption rate is largely controlled by the occupation of multiple active sites. Notably, the q_e determined from kinetic models was higher in the constant pH scenario (8.663 mg g^{-1}) compared to unregulated pH (4.480 mg g^{-1}). Conversely, adsorption isotherm analysis indicated that the Langmuir model best described the equilibrium data under constant pH conditions, yielding a higher q_{max} of 20.57 mg g^{-1} compared to 11.24 mg g^{-1} for unregulated pH. The R_L values, being consistently below 1, confirmed that the adsorption process is favorable and spontaneous under both regulated and unregulated pH conditions. The Freundlich model further supported adsorption on a heterogeneous surface, with 1/n values between 0 and 1 affirming favorable adsorption. Thermodynamic investigations confirmed that the adsorption of MB onto BC-OP is a spontaneous and thermodynamically favorable process, as indicated by the negative values of ΔG°, which became more negative at higher temperatures. The positive values of ΔH° (2.21 kJ mol^{-1} for unregulated pH, 4.88 kJ mol^{-1} for constant pH) confirmed the endothermic nature of the process, suggesting an energy input is required for optimal interaction. Furthermore, the magnitude of ΔH° (< 40 kJ mol^{-1}) strongly supports a physisorption-dominated mechanism, involving electrostatic interactions, π–π interactions, n-

π interactions, Van der Waals forces, and hydrogen bonds. The positive values of ΔS° further indicated an increase in molecular disorder at the adsorbent-adsorbate interface, promoting spontaneity.

We can conclude that the biochar derived from OPs through MAP represents a promising, effective, and sustainable adsorbent material for the removal of MB from wastewater, aligning with principles of a circular economy and addressing critical environmental challenges.

Supplementary Information

The supplementary materials are attached to this manuscript.

Data availability statement:

The datasets used and/or analyzed during the current study are available from the corresponding author on reasonable request.

Credit authorship contribution statement

Ullrich Stahl: Writing – review & editing, Writing – original draft, Methodology, Investigation, Formal analysis. Elvia V. Cabrera and Jhonny Correa-Abril: Writing – review & editing, Validation, Supervision, Formal analysis, Conceptualization. Nilo Robles: Writing, Validation, Supervision, Formal analysis, J. L. López Terán: Project administration, Funding acquisition.

Acknowledgments

The authors would like to express their gratitude to all the individuals and institutional collaborators who have provided their support and assistance and to the Universidad Central del Ecuador for financing the Senior Project DI-CONV-2022-025 and DI-CONV-2023-029. We are also very grateful to Dr. Carsten Natzeck from the Institute of Functional Interfaces – Karlsruhe Institute of Technology for his valuable support on SEM images and EDX analysis, the laboratory of research activities (LISE) of the Faculty of Chemical Engineering, as well as to Dr. Pablo Bonilla of the laboratory of nanomaterials of the Faculty of Chemistry for his support on ZP measurements.

Funding:

This work was financed by the Universidad Central del Ecuador and it´s Dirección de Investigación via the Senior Project "Desarrollo de un adsorbente basado en biocarbón de

Theobroma cacao y marco metal orgánico (MOF) para la remoción de fármacos en aguas residuales sintéticas" (No. DI-CONV-2023-029).

Declaration of interests

The authors declare that they have no known competing financial interests or personal relationships that could have appeared to influence the work reported in this paper.

References

1. Lin, J. et al. Environmental impacts and remediation of dye-containing wastewater. *Nat. Rev. Earth Environ.* **4**, 785–803 (2023).
2. Dutta, S. et al. Contamination of textile dyes in aquatic environment: Adverse impacts on aquatic ecosystem and human health, and its management using bioremediation. *J. Environ. Manage.* **353**, 120103 (2024).
3. Kobylewski, S. & Jacobson, M. F. Toxicology of food dyes. *Int. J. Occup. Environ. Health* **18**, 220–246 (2012).
4. Khan, I. et al. Review on Methylene Blue: Its Properties, Uses, Toxicity and Photodegradation. *Water* **14**, 242 (2022).
5. Kurniasih, M., Aprilita, N. H., Roto, R. & Mudasir, M. Modification of coal fly ash for high capacity adsorption of methylene blue. *Case Stud. Chem. Environ. Eng*. **11**, 101101 (2025).
6. Al-Tohamy, R. et al. A critical review on the treatment of dye-containing wastewater: Ecotoxicological and health concerns of textile dyes and possible remediation approaches for environmental safety. Ecotoxicol. *Environ. Saf.* **231**, 113160 (2022).
7. León, M., Silva, J., Carrasco, S. & Barrientos, N. Design, Cost Estimation and Sensitivity Analysis for a Production Process of Activated Carbon from Waste Nutshells by Physical Activation. *Processes* **8**, 945 (2020).
8. Jagadeesh, N. & Sundaram, B. Adsorption of Pollutants from Wastewater by Biochar: A Review. *J. Hazard. Mater. Adv*. **9**, 100226 (2023).

9. Michael-Igolima, U., Abbey, S. J., Ifelebuegu, A. O. & Eyo, E. U. Modified Orange Peel Waste as a Sustainable Material for Adsorption of Contaminants. *Materials* **16**, 1092 (2023).
10. Ayala, J. R. et al. Characterization of Orange Peel Waste and Valorization to Obtain Reducing Sugars. *Molecules* **26**, 1348 (2021).
11. Chen, Z. et al. Enhanced adsorption of phosphate on orange peel-based biochar activated by Ca/Zn composite: Adsorption efficiency and mechanisms. Colloids Surf. Physicochem. Eng. Asp. **651**, 129728 (2022).
12. Afolabi, F. O. & Musonge, P. Synthesis, Characterization, and Biosorption of Cu2+ and Pb2+ Ions from an Aqueous Solution Using Biochar Derived from Orange Peels. *Molecules* **28**, 7050 (2023).
13. Potnuri, R. et al. A review on analysis of biochar produced from microwave-assisted pyrolysis of agricultural waste biomass. *J. Anal. Appl. Pyrolysis* **173**, 106094 (2023).
14. Shirvanimoghaddam, K. et al. Microwave synthesis of biochar for environmental applications. *J. Anal. Appl. Pyrolysis* **161**, 105415 (2022).
15. Zhang, Y., Fan, S., Liu, T., Fu, W. & Li, B. A review of biochar prepared by microwave-assisted pyrolysis of organic wastes. *Sustain. Energy Technol. Assess.* **50**, 101873 (2022).
16. Ethaib, S., Omar, R., Kamal, S. M. M., Awang Biak, D. R. & Zubaidi, S. L. Microwave-Assisted Pyrolysis of Biomass Waste: A Mini Review. *Processes* **8**, 1190 (2020).
17. Lam, S. S. et al. Activated Carbon for Catalyst Support from Microwave Pyrolysis of Orange Peel. *Waste Biomass Valorization* **8**, 2109–2119 (2017).
18. Jawad, A. H., Hapiz, A., Wu, R. & ALOthman, Z. A. Mixed fruit Citrullus lanatus and Citrus sinensis wastes for mesoporous activated carbon via microwave assisted H3PO4 activation: Optimization for methylene blue dye removal. Biomass Convers. *Biorefinery* **15**, 6989–7003 (2025).

19. Correa-Abril, J. et al. Adsorption dynamics of Cd2+(aq) on microwave-synthetized pristine biochar from cocoa pod husk: Green, experimental, and DFT approaches. *iScience* **27**, (2024).
20. Zambrano-Intriago, L. et al. Kinetics, equilibrium, and thermodynamics of the blue 19 dye adsorption process using residual biomass attained from rice cultivation. Biomass Convers. *Biorefinery* **12**, (2022).
21. Andrade, C. et al. Adsorption Behavior and Mechanism of Oxytetracycline on Rice Husk Ash: Kinetics, Equilibrium, and Thermodynamics of the Process. *Water. Air. Soil Pollut.* **231**, 103 (2020).
22. Jayakumar, M. et al. Comprehensive review on lignocellulosic biomass derived biochar production, characterization, utilization and applications. *Chemosphere* **345**, 140515 (2023).
23. Mirkarimi, S. M. R., Bensaid, S., Negro, V. & Chiaramonti, D. Review of methane cracking over carbon-based catalyst for energy and fuels. *Renew. Sustain. Energy Rev.* **187**, 113747 (2023).
24. You, X., Wang, R., Zhu, Y., Sui, W. & Cheng, D. Comparison of adsorption properties of a cellulose-rich modified rice husk for the removal of methylene blue and aluminum (III) from their aqueous solution. *Ind. Crops Prod.* **170**, 113687 (2021).
25. García, D. B., Sanchez, M. C., Bacigalupe, A., Escobar, M. M. & Mansilla, M. A. Chapter 14 - Green rubber composites. *in Green Sustainable Process for Chemical and Environmental Engineering and Science* (eds Altalhi, T. & Inamuddin) 273–312 (Elsevier, 2022). doi:10.1016/B978-0-323-99643-3.00008-5.
26. Al-Janabi, E. S. H. & Yasen, S. S. Determination of chemical composition and antioxidants of wheat flour, orange peel powder and manufactured biscuits. *AIP Conf. Proc.* **2839**, 060006 (2023).
27. Li, S. & Tasnady, D. Biochar for Soil Carbon Sequestration: Current Knowledge, Mechanisms, and Future Perspectives. *C* **9**, 67 (2023).

28. Duan, C. et al. A review on nitrogen transformation mechanism during biomass pyrolysis. *J. Anal. Appl. Pyrolysis* **184**, 106863 (2024).
29. Liu, H. et al. Emission control of NOx precursors during sewage sludge pyrolysis using an integrated pretreatment of Fenton peroxidation and CaO conditioning. *Fuel* **195**, 208–216 (2017).
30. Bakshi, S., Banik, C. & Laird, D. A. Estimating the organic oxygen content of biochar. *Sci. Rep.* **10**, 13082 (2020).
31. Mastalerz, M., Drobniak, A., Liu, B. & Sauer, P. E. Reflectance as an indicator of biochar permanence. *Int. J. Coal Geol.* **306**, 104809 (2025).
32. Chen, Y., Zhang, X., Chen, W., Yang, H. & Chen, H. The structure evolution of biochar from biomass pyrolysis and its correlation with gas pollutant adsorption performance. *Bioresour. Technol.* **246**, 101–109 (2017).
33. Nuryana, D. et al. Methylene Blue Removal Using Coconut Shell Biochar Synthesized Through Microwave-Assisted Pyrolysis. *J. Teknol. Sci. Eng.* **82**, (2020).
34. Xia, Y., Yao, Q., Zhang, W., Zhang, Y. & Zhao, M. Comparative adsorption of methylene blue by magnetic baker's yeast and EDTAD-modified magnetic baker's yeast: Equilibrium and kinetic study. *Arab. J. Chem.* **12**, 2448–2456 (2015).
35. Afolabi, F. O., Musonge, P. & Bakare, B. F. Adsorption of Copper and Lead Ions in a Binary System onto Orange Peels: Optimization, Equilibrium, and Kinetic Study. *Sustainability* **14**, 10860 (2022).
36. Premalatha, R. P. et al. A review on biochar's effect on soil properties and crop growth. *Front. Energy Res.* **11**, (2023).
37. Geleto, M. A. et al. Influence of pyrolysis temperature and feedstock biomass on Cu2+, Pb2+, and Zn2+ sorption capacity of biochar. *Int. J. Environ. Sci. Technol.* **19**, 11857–11866 (2022).
38. Albalasmeh, A. et al. Characterization and Artificial Neural Networks Modelling of methylene blue adsorption of biochar derived from agricultural residues: Effect of

biomass type, pyrolysis temperature, particle size. *J. Saudi Chem. Soc.* **24**, 811–823 (2020).

39. Breen, R., Goggin, C., Holmes, J. D. & Collins, G. A Collaborative Cocurricular Undergraduate Research Experience on Sustainable Materials: Analysis of Biochar Using the Boehm Titration and Spectroscopic Techniques. *J. Chem. Educ.* **102**, 1323–1332 (2025).
40. Amalina, F., Razak, A. S. A., Krishnan, S., Zularisam, A. W. & Nasrullah, M. A comprehensive assessment of the method for producing biochar, its characterization, stability, and potential applications in regenerative economic sustainability – A review. *Clean. Mater.* **3**, 100045 (2022).
41. Barszcz, W., Łożyńska, M. & Molenda, J. Impact of pyrolysis process conditions on the structure of biochar obtained from apple waste. *Sci. Rep.* **14**, 10501 (2024).
42. Lam, S. S. et al. Microwave-assisted pyrolysis with chemical activation, an innovative method to convert orange peel into activated carbon with improved properties as dye adsorbent. *J. Clean. Prod.* **162**, 1376–1387 (2017).
43. Ho, Y. S. & McKay, G. Pseudo-second order model for sorption processes. *Process Biochem.* **34**, 451–465 (1999).
44. Ahmaruzzaman, M. & Gupta, V. K. Rice Husk and Its Ash as Low-Cost Adsorbents in Water and Wastewater Treatment. *Ind. Eng. Chem. Res.* **50**, 13589–13613 (2011).
45. Dotto, J., Fagundes-Klen, M. R., Veit, M. T., Palácio, S. M. & Bergamasco, R. Performance of different coagulants in the coagulation/flocculation process of textile wastewater. *J. Clean. Prod.* **208**, 656–665 (2019).
46. Sukor, N. F. & Jusoh, R. Hybrid activated carbon/ maltodextrin-functionalized fibrous silica for acetaminophen and amoxicillin adsorption: Advanced statistical physics modelling. *Environ. Res.* **278**, 121691 (2025).
47. Al-Harby, N. F., Albahly, E. F. & Mohamed, N. A. Kinetics, Isotherm and Thermodynamic Studies for Efficient Adsorption of Congo Red Dye from Aqueous Solution onto Novel Cyanoguanidine-Modified Chitosan Adsorbent. *Polymers* **13**, 4446 (2021).

48. Liu, B. *et al.* Temperature-induced adsorption and desorption of phosphate on poly(acrylic acid-co-N-[3-(dimethylamino)propyl]acrylamide) hydrogels in aqueous solutions. *Desalination Water Treat.* **160**, 260–267 (2019).
49. Kumar, M. & Tamilarasan, R. Kinetics, equilibrium data and modeling studies for the sorption of chromium by Prosopis juliflora bark carbon. *Arab. J. Chem.* **10**, S1567–S1577 (2013).
50. Ao, C. *et al.* Impact of External Conditions on the Desorption and Degradation Capacity of Biochar for Rhodamine B. *Molecules* **30**, 1717 (2025).
51. Maaoui, A. *et al.* Calcium-Rich Biochar Derived from Cactus Feedstock and Its Efficient Adsorption Properties for Industrial Dye. *Appl. Sci.* **15**, 894 (2025).
52. Saha, N. *et al.* Cationic Dye Adsorption on Hydrochars of Winery and Citrus Juice Industries Residues: Performance, Mechanism, and Thermodynamics. *Energies* **13**, 4686 (2020).
53. Tenea, A.-G. *et al.* Exploring adsorption dynamics of heavy metals onto varied commercial microplastic substrates: Isothermal models and kinetics analysis. *Heliyon* **10**, e35364 (2024).
54. Ren, Y., Geng, W., Xu, R., Wang, P. & Zhao, H. Tuning Electronic and Pore Structures of Biochar via Nitrogen and Magnesium Doping for Superior Methylene Blue Adsorption: Synergistic Mechanisms and Kinetic Analysis. *ACS Omega* **10**, 31679–31692 (2025).
55. Chu, K. H. *et al.* The Redlich–Peterson isotherm for aqueous phase adsorption: Pitfalls in data analysis and interpretation. *Chem. Eng. Sci.* **285**, 119573 (2024).
56. Hanafi, N. A. M. *et al.* Optimized removal process and tailored adsorption mechanism of crystal violet and methylene blue dyes by activated carbon derived from mixed orange peel and watermelon rind using microwave-induced ZnCl2 activation. *Biomass Convers. Biorefinery* **14**, 28415–28427 (2024).
57. Amin, M. T., Alazba, A. A. & Shafiq, M. Comparative study for adsorption of methylene blue dye on biochar derived from orange peel and banana biomass in aqueous solutions. *Environ. Monit. Assess.* **191**, 735 (2019).

58. Gunay Gurer, A., Aktas, K., Ozkaleli Akcetin, M., Erdem Unsar, A. & Asilturk, M. Adsorption Isotherms, Thermodynamics, and Kinetic Modeling of Methylene Blue onto Novel Carbonaceous Adsorbent Derived from Bitter Orange Peels. *Water. Air. Soil Pollut.* **232**, 138 (2021).
59. Ding, W. *et al.* Environmental applications of lignin-based hydrogels for Cu remediation in water and soil: adsorption mechanisms and passivation effects. *Environ. Res.* **250**, 118442 (2024).
60. Zaheer, Z., AbuBaker Bawazir, W., Al-Bukhari, S. M. & Basaleh, A. S. Adsorption, equilibrium isotherm, and thermodynamic studies to the removal of acid orange 7. *Mater. Chem. Phys.* **232**, 109–120 (2019).
61. Huang, Y.-T. & Shih, M.-C. Kinetic, Isotherm, and Thermodynamic Modeling of Methylene Blue Adsorption Using Natural Rice Husk: A Sustainable Approach. *Separations* **12**, 189 (2025).
62. Garcia, E. M., Taroco, H. A. & Melo, J. O. F. Highly efficient Eugenia dysenterica DC seeds biomass as adsorbent for methylene blue removal. *Discov. Chem.* **2**, 11 (2025).
63. El-Rayyes, A. *et al.* Thermodynamic, isotherm and kinetic studies lead ions adsorption onto Manihot esculenta chaff surface. *Sci. Rep.* **15**, 27672 (2025).
64. Salgın, U., Alomari, İ., Soyer, N. & Salgın, S. Adsorption of Bisphenol A onto β-Cyclodextrin–Based Nanosponges and Innovative Supercritical Green Regeneration of the Sustainable Adsorbent. *Polymers* **17**, 856 (2025).
65. Xiang, L. *et al.* Potential hazards of biochar: The negative environmental impacts of biochar applications. *J. Hazard. Mater.* **420**, 126611 (2021).